*J. Fluid Mech.* (2001), *vol.* 442, *pp.* 267–291. Printed in the United Kingdom



# Measurements of diapycnal diffusivities in stratified fluids

By MICHAEL E. BARRY[1], GREGORY N. IVEY[1], KRAIG B. WINTERS[2] AND JÖRG IMBERGER[1]

[1]Centre for Water Research, The University of Western Australia, Crawley 6009, Australia
[2]Applied Physics Laboratory, University of Washington, Seattle WA 98105-6698, USA

(Received 3 July 2000 and in revised form 16 March 2001)

Linearly stratified salt solutions of different Prandtl number were subjected to turbulent stirring by a horizontally oscillating vertical grid in a closed laboratory system. The experimental set-up allowed the independent direct measurement of a root mean square turbulent lengthscale $L_t$, turbulent diffusivity for mass $K_\rho$, rate of dissipation of turbulent kinetic energy $\epsilon$, buoyancy frequency $N$ and viscosity $\nu$, as time and volume averaged quantities. The behaviour of both $L_t$ and $K_\rho$ was characterized over a wide range of the turbulence intensity measure, $\epsilon/\nu N^2$, and two regimes were identified.

In the more energetic of these regimes (Regime E, where $300 < \epsilon/\nu N^2 < 10^5$), $L_t$ was found to be a function of $\nu$, $\kappa$ and $N$, whilst $K_\rho$ was a function of $\nu, \kappa$ and $(\epsilon/\nu N^2)^{1/3}$. From these expressions for $L_t$ and $K_\rho$, a scaling relation for the root mean square turbulent velocity scale $U_t$ was derived, and this relationship showed good agreement with direct measurements from other data sets.

In the weaker turbulence regime (Regime W, where $10 < \epsilon/\nu N^2 < 300$) $K_\rho$ was a function of $\nu, \kappa$ and $\epsilon/\nu N^2$.

For $10 < \epsilon/\nu N^2 < 1000$, our directly measured diffusivities, $K_\rho$, are approximately a factor of 2 different to the diffusivity predicted by the model of Osborn (1980). For $\epsilon/\nu N^2 > 1000$, our measured diffusivities diverge from the model prediction. For example, at $\epsilon/\nu N^2 \approx 10^4$ there is at least an order of magnitude difference between the measured and predicted diffusivities.

## 1. Introduction

A clear understanding of the irreversible vertical transport of mass in a stably stratified turbulent flow is fundamental to quantifying the dynamics of density stratified fluids. The rate at which this transport occurs has historically been modelled as a turbulent diffusivity for mass, $K_\rho$. Since $K_\rho$ influences the rate at which heat, mass, contaminants and biota are distributed throughout a turbulent fluid (Tennekes & Lumely 1972), an understanding of this quantity is essential to the management of aquatic systems such as lakes, estuaries and the oceans. Field experiments have been undertaken that estimate $K_\rho$ in lakes and oceans by using both tracer and microstructure techniques (e.g. Ledwell, Watson & Law 1993; Wuest *et al.* 1996; Polzin *et al.* 1997; Ledwell *et al.* 2000). These experiments, however, have typically spanned a small range of turbulence intensities. No controlled laboratory or field experiments have been executed that directly measure $K_\rho$ and quantitatively describe it in terms

of routinely measured fluid and flow properties over a wide range of turbulence intensities. The current work addresses this issue.

As a result of its importance in ecological applications, a number of models describing the rate of turbulent transport have been proposed. We review some of these models here.

### 1.1. *Bulk eddy diffusivity*

The simplest model describing turbulent transport in homogeneous isotropic turbulence relates a turbulent diffusivity $K$ to a turbulent velocity scale $U$ and a turbulent integral lengthscale $L$ (Tennekes & Lumely 1972),

$$K \sim UL. \tag{1.1}$$

This expression for $K$ is considered to represent a bulk eddy diffusivity. Taylor (1935) found that for an unstratified fluid, the rate of dissipation of turbulent kinetic energy per unit mass, $\epsilon$, scales like,

$$\epsilon \sim \frac{u^3}{l}, \tag{1.2}$$

where $u$ is the fluctuating component of velocity and $l$ is a linear dimension defining the scale of the turbulent field. This result has been confirmed by Ivey, Imberger & Koseff (1998) for a stratified fluid. If we assume that $U, L, u$ and $l$ are well represented by their root mean square velocity and lengthscales $U_t$ and $L_t$ respectively, (1.1) and (1.2) can be combined to give (Richardson 1926; Monin & Yaglom 1971),

$$K \sim \epsilon^{1/3} L_t^{4/3}. \tag{1.3}$$

In stratified geophysical flows, one of the diffusivities of interest is $K_\rho$, which has typically been modelled as a scalar flux normalized by a scalar gradient (e.g. Osborn 1980; Winters & D'Asaro 1996),

$$K_\rho = \frac{\text{flux}}{\text{gradient}}. \tag{1.4}$$

It is differences in the definitions of the quantities chosen to represent these flux and gradient terms that distinguish most models for $K_\rho$. We discuss some of these models based on this distinction.

### 1.2. *Average buoyancy flux to model $K_\rho$*

Currently, the most widely used model for estimating $K_\rho$ in geophysical flows is that due to Osborn (1980). This model applies the turbulent kinetic energy equation (e.g. Stull 1994, where the viscous transport of turbulent kinetic energy has been neglected) to the ocean thermocline,

$$-\frac{\partial \bar{e}}{\partial t} - \overline{U_j}\frac{\partial \bar{e}}{\partial x_j} - \overline{u_i' u_j'}\frac{\partial \overline{U_i}}{\partial x_j} - \frac{\partial(\overline{u_j' e})}{\partial x_j} - \frac{1}{\rho_0}\frac{\partial(\overline{u_i' p'})}{\partial x_i} = \delta_{i3}\frac{g}{\rho_0}(\overline{u_i' \rho'}) + \epsilon, \tag{1.5}$$

where $\bar{e} = 0.5(\overline{u_1'^2} + \overline{u_2'^2} + \overline{u_3'^2})$ is the turbulent kinetic energy per unit mass, $u_i'$ is the fluctuating velocity in the $i$th direction, $\rho_0$ is a reference density, $\epsilon = \nu(\overline{\partial u_i'/\partial x_j})^2$ is the rate of dissipation of turbulent kinetic energy per unit mass, $\nu$ is the kinematic viscosity, the velocity component $u_3$ is vertically upward, and the overbar signifies a time, space or ensemble average. Osborn (1980) applied (1.5) to the ocean thermocline, and assumed (i) steady flow, (ii) no spatial gradients of turbulent kinetic energy,

and (iii) both the pressure velocity correlation and turbulent diffusion terms to be negligible. These assumptions simplify (1.5) to,

$$S_p = -b + \epsilon, \tag{1.6}$$

where $S_p$ is the production of turbulent kinetic energy due only to shear in the mean flow $(-(\overline{u_i' u_j'})\partial \overline{U_i}/\partial x_j)$ and $b$ is the average of the instantaneous vertical advective flux, or buoyancy flux, $-g(\overline{u_3' \rho'})/\rho_0$ (Winter & D'Asaro 1996). Osborn (1980) defined $K_\rho$ in the form of (1.4) as,

$$K_\rho = -\frac{b}{N^2}, \tag{1.7}$$

where $N^2 = -(g/\rho_0)(\mathrm{d}\bar{\rho}/\mathrm{d}z)$ and $\mathrm{d}\bar{\rho}/\mathrm{d}z$ is the mean vertical density gradient. By introducing a flux Richardson number,

$$R_f = -\frac{b}{S_p}, \tag{1.8}$$

Osborn (1980) expressed $K_\rho$ as,

$$K_\rho = \left(\frac{R_f}{1 - R_f}\right)\frac{\epsilon}{N^2}. \tag{1.9}$$

Using the theoretical result of Ellison (1957) to set an upper bound of $R_f = 0.15$, Osborn (1980) predicted $K_\rho$ in the ocean thermocline,

$$K_\rho \leqslant 0.2\frac{\epsilon}{N^2}. \tag{1.10}$$

This model assumes that $b$ captures the physics of turbulent mixing. As a result, much attention has been focused on the behaviour of $b$. For instance, a number of laboratory experiments (Stillinger, Helland & Van Atta 1983; Itsweire, Helland & Van Atta 1986; Rohr *et al.* 1988; Ivey & Nokes 1989; Lienhard & Van Atta 1990) have investigated the extinction of $b$ and thus, by inference from (1.7), the cessation of turbulent mixing. Gibson (1980) suggested that this extinction point is described by,

$$\epsilon_F \sim \nu N^2, \tag{1.11}$$

where $\epsilon_F$ is the viscous dissipation rate at the extinction of $b$. The results of the above laboratory studies suggested that the constant of proportionality in (1.11) is approximately 15. By implication of (1.7), $K_\rho$ is presumed to revert to molecular levels when $\epsilon < 15\nu N^2$ (Ivey, Winters & De Silva 2000).

Using the experimental data of Stillinger *et al.* (1983), Itsweire *et al.* (1986), Rohr *et al.* (1988) and Lienhard & Van Atta (1990), Ivey & Imberger (1991) suggested that $b$ can be evaluated directly in terms of $\epsilon$, $N$, $\nu$ and $L_C$, where $L_C$ is a centred displacement scale describing the scale of the turbulent overturns. Recently, $b$ has been measured directly both in field and laboratory applications (e.g. Moum 1990; Ivey *et al.* 2000; Saggio & Imberger 2001). It has been found that the interpretation of $b$ is not always clear (e.g. Imberger 1994, 1998), as an instantaneous measurement of $\rho' w'$ can be as frequently negative as it is positive (Moum 1990). With a very large data set, however, Saggio & Imberger (2001) found a detectable difference in the positive and negative instantaneous advective flux for $\epsilon/\nu N^2 \geqslant 36$, where $\overline{\rho' w'} > 0$.

Ivey *et al.* (2000) found laboratory measurements of $b$ difficult to interpret. They characterized turbulence with both a high dissipation rate (indicating a well-developed velocity cascade) and negligible $b$. If (1.7) holds, then $K_\rho$ is also negligible. This implies

that, whilst supporting an active velocity cascade, the turbulence in their experiments could not support a cascade of scalar variance to small scales where molecular diffusion occurs (Winters & Ivey 1999).

Lienhard & Van Atta (1990) found that the criterion $\overline{\theta' w'} = 0$ in temperature stratified flows in air was insufficient to characterize the extinction of active turbulence. Co-spectral analyses revealed that whilst globally $\overline{\theta' w'} = 0$, this was often due to masking of negative $\theta' w'$ at small scales by positive $\theta' w'$ induced by restratification at large scales.

### 1.3. *Diffusive flux to model $K_\rho$*

Winters & D'Asaro (1996) used an irreversible Fickian diffusive flux in (1.4) as an alternative to $b$. The diffusive flux, $\phi_d$, of a scalar $\theta$ across an isoscalar surface $S$ in a turbulent flow was expressed as,

$$\phi_d = \frac{1}{A}\int_S \kappa |\nabla\theta| \mathrm{d}S = \kappa \frac{\langle |\nabla\theta| \rangle_{z_*}^2}{|\mathrm{d}\theta/\mathrm{d}z_*|}, \tag{1.12}$$

where $z_*$ is an isoscalar coordinate with dimensions of length, the angle brackets indicate a spatial average over the surface $S$, $\kappa$ is the molecular diffusivity of the species and $A$ is the geometrical projection of the surface $S$ onto the horizontal. By normalizing $\phi_d$ against the magnitude of the resorted scalar gradient $|\mathrm{d}\rho/\mathrm{d}z_*|$, Winters & D'Asaro (1996) expressed $K_\rho$ as (in the form of (1.4)),

$$K_\rho = \frac{\phi_d}{|\mathrm{d}\rho/\mathrm{d}z_*|} = \kappa \frac{\langle |\nabla\rho| \rangle_{z_*}^2}{|\mathrm{d}\rho/\mathrm{d}z_*|^2}, \tag{1.13}$$

where (1.13) has been written with density as the scalar.

Ivey *et al.* (2000) applied scaling arguments to this result and suggested that (1.13) could be written as,

$$K_\rho \sim \left(\frac{L}{L_B}\right)^2 \kappa, \tag{1.14}$$

where $L$ is a characteristic displacement scale of the turbulent eddies and $L_B$ is the Batchelor scale (see table 1),

$$L_B = \kappa^{1/2}\left(\frac{\nu}{\epsilon}\right)^{1/4}. \tag{1.15}$$

Ivey *et al.* (2000) identified three turbulent regimes, each with characteristic $K_\rho$, from the laminar limit up to energetic density-stratified turbulence. With the exception of the laminar limit, it was hypothesized that $K_\rho$ was a function of $N^2$, $\epsilon$ and $\nu$ only. Ivey *et al.* (2000) made no formal prediction for $K_\rho$ when $\epsilon/\nu N^2 > 15$.

### 1.4. *Summary*

Several models have thus been proposed that predict $K_\rho$ in geophysical flows. The majority of models have expressed $K_\rho$ as a function of typically measured flow properties, so that,

$$K_\rho = K_\rho(\epsilon, N^2, L, \nu, \kappa), \tag{1.16}$$

where $L$ is some displacement scale of the turbulence (Imberger 1994). Whilst an advective buoyancy flux $b$ can now be measured directly, it is not a measurement that can be routinely made and its interpretation is often unclear (e.g. Imberger 1994; Moum 1996; Winters & Ivey 1999; Ivey *et al.* 2000). Currently, the most common model for $K_\rho$ in both field and laboratory situations is due to Osborn (1980) (see

| Lengthscale | Symbol | Definition | Interpretation |
|---|---|---|---|
| Characteristic r.m.s. | $L_t$ | $\overline{(T'^2)}^{1/2}/(\mathrm{d}\bar{T}/\mathrm{d}z)$ | The scale representative of the vertical turbulent excursion of a fluid particle |
| Ozmidov | $L_o$ | $(\epsilon/N^3)^{1/2}$ | The scale at which buoyancy forces balance inertial forces |
| Kolmogorov | $L_K$ | $(\nu^3/\epsilon)^{1/4}$ | The scale at which viscous forces balance inertial forces.<br>Velocity fluctuations cannot exist at scales smaller than the Kolmogorov scale |
| Batchelor | $L_B$ | $\kappa^{1/2}(\nu/\epsilon)^{1/4}$ | The scale at which molecular diffusion smooths locally enhanced scalar gradients |
| Convective | $L_{co}$ | $(\nu\kappa)^{1/4}/N^{1/2}$ | The scale which makes the Rayleigh number $Ra = N^2L^4/\nu\kappa$ constant |

TABLE 1. Description of turbulent lengthscales.

(1.10)). Often, the Osborn (1980) model is used as an equality, with some uncertainty in the selection of the constant coefficient (e.g. Wuest *et al.* 1996; Moum 1996).

Previous laboratory experiments have measured some of the quantities in (1.16) (e.g. Ivey & Nokes 1989; Ruddick, McDougall & Turner 1989; Park, Whitehead & Gnanadeskian 1994; Liu 1995; Rehmann 1995; Teoh, Ivey & Imberger 1997; Holford & Linden 1999; Ivey *et al.* 2000). However, no well-controlled experiments have been undertaken that independently measure the properties of the turbulence field and its consequences, i.e. $K_\rho$, and therefore that clearly and unambiguously define the relationship between $K_\rho$ and all the quantities given in (1.16) over a wide range of turbulence intensities. This is the purpose of the present work.

We describe the laboratory experiments in § 2 and present the turbulent lengthscale and turbulent diffusivity results in § 3, where we have measured $L$ as a root mean square (r.m.s.) quantity $L_t$. In § 3 we also propose general scaling relations for $L_t$, $K_\rho$ and $U_t$, where $U_t$ is an r.m.s. overturn velocity. In § 4 we discuss our results and offer an interpretation for the mechanism by which turbulent mixing occurs. We also compare and contrast our results with prior models of mixing in turbulent stratified fluids.

## 2. Experiments

### 2.1. *Experimental facility and instrumentation*

The experimental set-up is shown in figures 1 and 2. The apparatus consisted of a 520 mm long × 480 mm wide × 600 mm deep glass tank, filled with a linearly stratified salt solution to approximately 480 mm. Turbulence was generated by the horizontal motion of a rigid vertical grid (with overall dimensions 480 mm × 480 mm) mounted on a pneumatic drive. The grid comprised 10 mm square horizontal and vertical bars, at a spacing of 50 mm. Under the power of the pneumatic drive, this grid was able to move continually back and forth in the horizontal direction along the entire 520 mm length of the tank at a preselected constant velocity. The time required for this drive to accelerate the grid from rest to a constant speed was negligible.

Four instruments were employed to compute the quantities in (1.16). Vertical temperature and conductivity profiles were logged simultaneously at 100 Hz using a single Precision Measurement Engineering fast response FP07 thermistor and 4-electrode fast response conductivity probe (FRC), mounted on a vertical traverser.

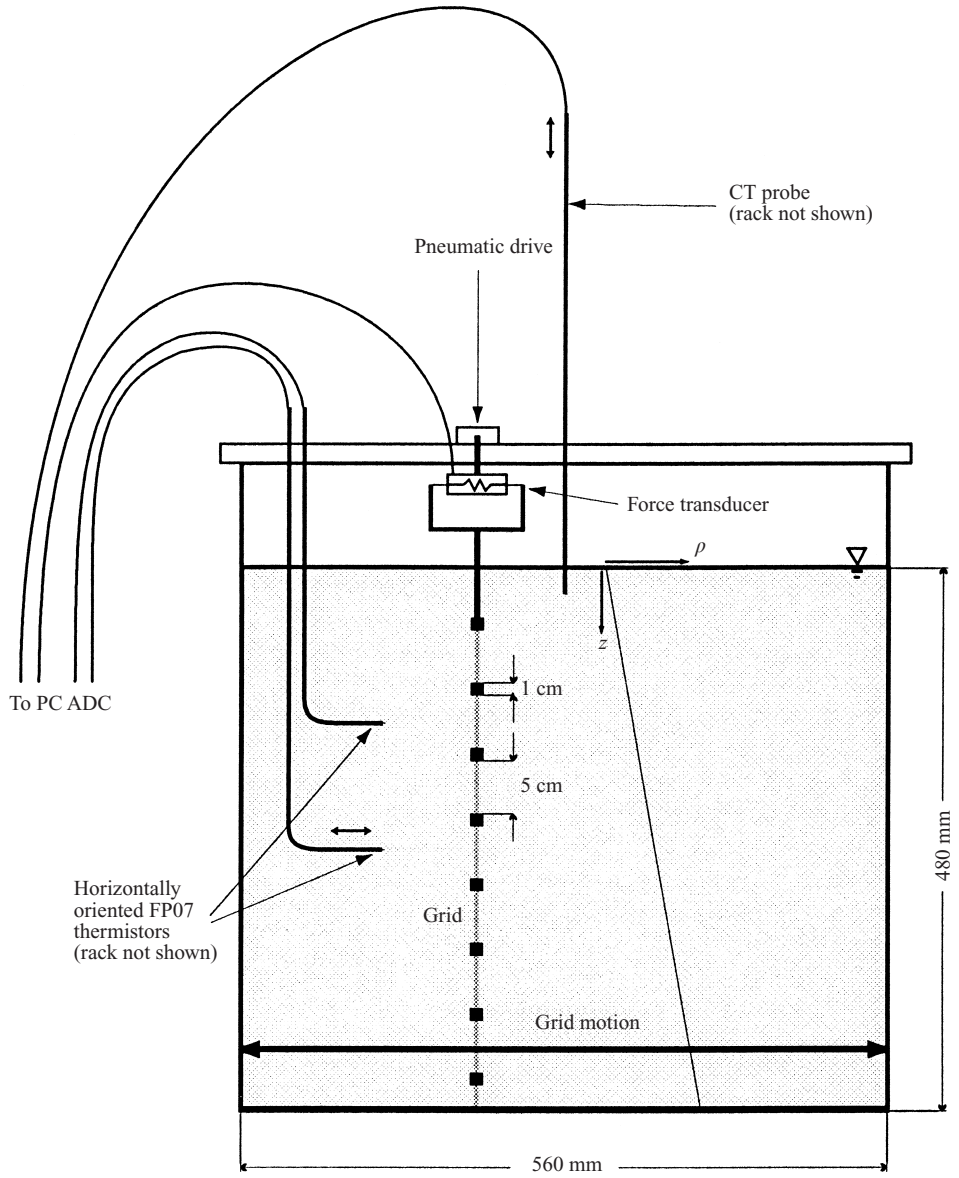


FIGURE 1. Schematic diagram of the side view of the experimental set-up. The vertical grid is driven in horizontal motion by the pneumatic drive, and grid motion is over the entire width of the tank.

The probe was constructed so that the tips of the temperature and conductivity sensors were 1 mm apart. A computer controlled stepping motor drove the traverser at a speed of 25 mm $s^{-1}$.

In addition, two L-shaped horizontally oriented fast response FP07 thermistors were mounted on a rack such that they could be traversed horizontally at any height along the tank in the direction of the grid motion. This set-up also allowed the thermistors to remain stationary. A 15 mm wide portion of the horizontal bars was removed down a vertical axis in the centre of the grid to allow the free motion of these thermistors. All FP07 resistances and the FRC current were converted to

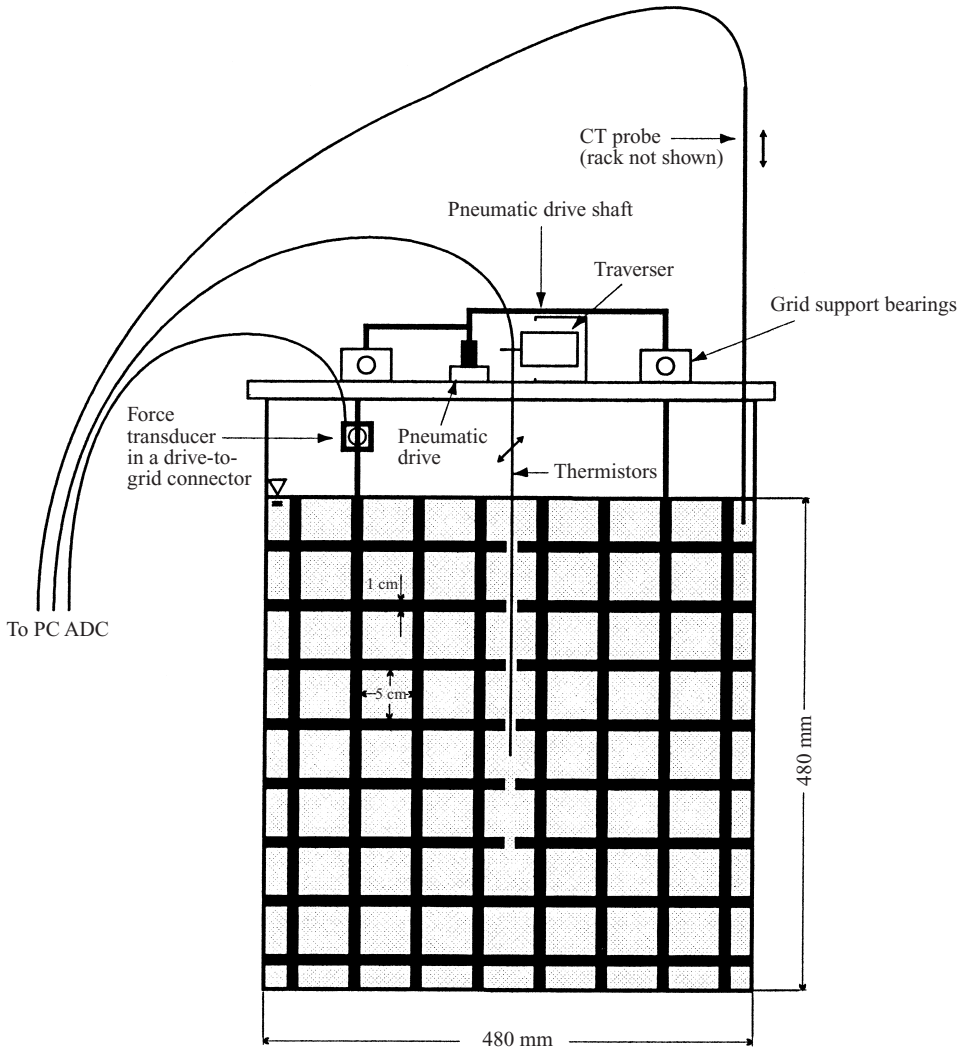


FIGURE 2. Schematic diagram of the front view of the experimental set-up. During grid motion, the signals from the thermistors and the force transducer are logged. The CT probe is used to sample the density gradient when the grid motion has ceased.

output voltages in a conditioning box, then digitized at 100 Hz using a 16 bit RTI850 analogue-to-digital converter (ADC).

A force transducer was mounted on the apparatus such that it was the sole active link between the pneumatic drive and the grid. The force transducer voltage was logged directly at 10 Hz using a separate acquisition system employing a 12 bit Data Translation DT2801A ADC.

Both water and water–glycerol solutions were used as the working fluids in the experiments (see § 2.2). The absolute viscosity, $\mu$, of the water–glycerol solution was measured at an average salinity using a Haake Viscotester, VT550, incorporating a Haake Sensor System PK100D. The absolute viscosity was measured at a rotation rate of 800 revolutions per second and a temperature of 22 °C, and then converted to kinematic viscosity.

### 2.2. *Experimental procedure*

The tank was filled with a linearly stratified salt solution to a depth of approximately 480 mm. The depth of the fluid was usually slightly greater ($< 20$ mm) than the grid height. This allowed the FRC to remain continually submerged throughout an experiment and to maintain adequate clearance from the grid. During the filling process, a small mean vertical temperature gradient was intentionally introduced into the working fluid. This was achieved by allowing the water in the supply tanks to recirculate through a pumping system. This gradient provided an additional diagnostic tool to describe the turbulence generated by the grid motion (see § 2.3). Compared to an equivalently salt stratified isothermal fluid at room temperature, the average density anomaly due to this temperature gradient was less than 2.0% of that due to the salinity. This ensured that the introduced temperature gradient was dynamically insignificant.

Initially, after all fluid motions resulting from the filling process had dissipated, a vertical conductivity and temperature profile of the fluid was taken using the vertically mounted FP07/FRC probe. The fluid density was then computed using the equations of Ruddick & Shirtcliffe (1979). After waiting sufficient time for the wake from this first traverse to dissipate, a second traverse was taken. Oscillatory grid motion was then initiated at a preselected constant grid speed $U_g$ to generate turbulence in the fluid. During this time, the time series signals from the force transducer and the horizontally oriented thermistors were logged. For all the experiments, the horizontally oriented thermistors were kept stationary. The duration of grid motion was usually of the order of five minutes, depending on the stratification strength. We refer to this active mixing time as a single mixing event.

At the termination of a mixing event, residual turbulent and internal wave motions in the fluid were allowed to decay. After this time, the vertical conductivity and temperature profiles were twice re-sampled in the same manner as before the mixing event. Grid motion was then recommenced and the thermistor and force transducer signals again collected for this new mixing event. The above routine was then repeated several times, with up to ten individual mixing events constituting an overall experiment.

Ten experiments were executed in total. Experiments 1 to 8 were conducted in salt stratified water. In order to observe the effect of varying Prandtl number (where we refer to the Prandtl number as the ratio of the kinematic viscosity of the working fluid to the molecular diffusivity of the stratifying species), the final two experiments used a 50% by weight water–glycerol solution as the working fluid, in place of pure water. A linear salt stratification was then constructed in the experimental tank using this solution. A summary of the initial conditions for all experiments is shown in table 2.

### 2.3. *Measurement of the r.m.s. turbulent lengthscale, $L_t$*

The r.m.s. turbulent lengthscale, $L_t$, was computed from the stationary thermistor time-series record. After filtering the record to remove internal wave contributions, an r.m.s. temperature fluctuation was computed, and divided by the local vertical temperature gradient,

$$L_t = \frac{\left(\overline{T'^2}\right)^{1/2}}{(\mathrm{d}\bar{T}/\mathrm{d}z)}. \tag{2.1}$$

Although the vertical temperature gradient was small (§ 2.2), it was sufficient to resolve adequately both the numerator and denominator in (2.1). One estimate of $L_t$ was

| Experiment number | $N^2$ (rad$^2$ s$^{-2}$) | $U_g$ (mm s$^{-1}$) |
|---|---|---|
| 1 | 0.0945 | 74 |
| 2 | 0.1415 | 74 |
| 3 | 0.0217 | 90 |
| 4 | 0.3631 | 45 |
| 5 | 0.5501 | 70 |
| 6 | 0.8423 | 70 |
| 7 | 0.5015 | 52 |
| 8 | 1.1943 | 42 |
| 9 | 0.0569 | 82 |
| 10 | 0.1139 | 75 |

TABLE 2. Initial experimental conditions. Experiments 9 and 10 were conducted in an approximately 50% by weight water–glycerol solution. $N^2 = -(g/\rho_0)(\mathrm{d}\rho/\mathrm{d}z)$ where $\mathrm{d}\rho/\mathrm{d}z$ is the initial density gradient. $U_g$ is the preselected constant grid velocity.

computed using (2.1) from each thermistor, and these were then averaged to yield a single time and volume averaged estimate of $L_t$ for each mixing event. Precision Measurement Engineering FRCs were not used to measure $L_t$ as these probes operate optimally under mean flow conditions when fluid velocities are oriented along the probe axis. Under zero mean flow conditions, such as in our experimental tank, the FRCs have reduced response characteristics and were not suitable for our purposes.

### 2.4. *Measurement of* $K_\rho$

In a closed stratified system, a turbulent diffusivity $K_\rho$ will manifest itself as a temporal change in the system's background potential energy, $E_b$, where $E_b$ is the minimum potential energy attainable through adiabatic redistribution of $\rho$. These experiments were designed to sample the density profile only after allowing the fluid to re-sort itself adiabatically after a mixing event (§ 2.2). Thus, the potential energy computed from this re-sorted profile is the background potential energy $E_b$, and the time rate of change of this quantity was used to directly compute $K_\rho$,

$$K_\rho = \frac{\left(Ag\int_0^H \rho z \mathrm{d}z\right)_{final} - \left(Ag\int_0^H \rho z \mathrm{d}z\right)_{initial}}{Vg\Delta t(\mathrm{d}\rho/\mathrm{d}z)_{average}} = \frac{\Delta E_b}{Vg\Delta t(\mathrm{d}\rho/\mathrm{d}z)_{average}}, \tag{2.2}$$

where $A$ is the horizontal area of the tank, $V$ is the volume of the fluid, $\Delta t$ is the duration of the mixing event and $(\mathrm{d}\rho/\mathrm{d}z)_{average}$ is the average background density gradient computed from the density gradients prior and subsequent to a mixing event (see Appendix). In the current experiments, changes in the background temperature field (see § 2.2) typically contributed less than 4% to $\Delta E_b$. Winters *et al.* (1995) showed that at any time in a closed system, the rate of change of $E_b$ is equal to the instantaneous, volume-integrated, irreversible diffusive flux $\Phi_d$,

$$\frac{\mathrm{d}}{\mathrm{d}t}E_b = \Phi_d. \tag{2.3}$$

In the current experiments we measured the change in $E_b$ over a mixing event of finite duration $\Delta t$. We define a time and volume-integrated irreversible diffusive flux

$\bar{\Phi}_d$ for each mixing event as,

$$\bar{\Phi}_d = \frac{1}{\Delta t}\int_0^{\Delta t} \Phi_d(t')\mathrm{d}t', \tag{2.4}$$

where $t'$ is a variable of integration. Integrating (2.3) from 0 to $\Delta t$ gives,

$$\Delta E_b = \int_0^{\Delta t} \Phi_d(t')\mathrm{d}t' = \Delta t\bar{\Phi}_d, \tag{2.5}$$

or,

$$\frac{\Delta E_b}{\Delta t} = \bar{\Phi}_d, \tag{2.6}$$

where $\Delta E_b$ is the change in background potential energy over the mixing time $\Delta t$. Hence, (2.2) can be rewritten,

$$K_\rho = \frac{\bar{\Phi}_d}{Vg(\mathrm{d}\rho/\mathrm{d}z)_{average}}. \tag{2.7}$$

The definition in (2.7) is of the same form as (1.4), and allowed the computation of a volume and time-averaged $K_\rho$.

### 2.5. *Measurement of dissipation*

The rate of dissipation of turbulent kinetic energy, $\epsilon$, was calculated by considering a power balance in the experimental system. The sole power input to the fluid was that resulting from the oscillatory motion of the vertical grid. Since the drag force of the fluid on the grid, $F_D$, was measured directly with a force transducer (§ 2.1), and the grid velocity, $U_g$, was constant for each experiment, the time-averaged power input per unit volume was computed as,

$$\text{Power input} = \sigma \times F_D \times U_g, \tag{2.8}$$

where $\sigma$ is the grid solidity (equal to the cross-sectional area occupied by the grid bars divided by the total cross-sectional area of the grid) and $U_g$ is the grid velocity. Over the course of one mixing event, the only energy sinks available in the flow were losses to dissipation and irreversible potential energy changes, such that

$$\sigma \times F_D \times U_g = \epsilon \times \text{mass} + \frac{\Delta E_b}{\Delta t}. \tag{2.9}$$

Dissipation was computed via (2.9), since all other quantities were measured directly, and the mass of fluid was computed from the background density profile. This measurement of $\epsilon$ is a time- and volume-averaged quantity.

In order to compute the above quantities, measurements of $\Delta t$, $F_D$ and $\mathrm{d}\rho/\mathrm{d}z$ were required. Details of their measurement and processing are given in the Appendix, together with some discussion on the influence of internal waves on the experiments.

### 2.6. *Averaged advective buoyancy flux*

With the current set-up and procedure, we can also infer a time- and volume-averaged advective buoyancy flux in these experiments. The instantaneous volume integrated advective buoyancy flux $\Phi_z$ is given by,

$$\Phi_z = g\int_V \rho w \mathrm{d}V, \tag{2.10}$$

where $\rho$ is the Boussinesq density and $w$ the vertical fluid velocity (Winters *et al.* 1995). This advective flux is related to $\Phi_d$ such that,

$$\frac{\mathrm{d}}{\mathrm{d}t}E_a = \Phi_z - \Phi_d + \Phi_i, \tag{2.11}$$

where $E_a$ is the potential energy released in the adiabatic transition of a density field to its resorted state and $\Phi_i$ is the instantaneous rate of conversion of internal to potential energy. Following the same approach given in § 2.4, we can integrate (2.11) from 0 to $\Delta t$ to give,

$$\frac{\Delta E_a}{\Delta t} = \bar{\Phi}_z - \bar{\Phi}_d + \bar{\Phi}_i, \tag{2.12}$$

where the overbars signify averages of $\Phi_z$ and $\Phi_i$ defined in the same way as $\bar{\Phi}_d$ in (2.4). In these experiments, $\bar{\Phi}_i$ was typically less that 0.06% of $\bar{\Phi}_d$, so it is neglected. Since vertical profiles were only taken once the fluid had relaxed to its re-sorted state, $E_a = \Delta E_a = 0$ by construction. Hence, (2.12) collapses to,

$$\bar{\Phi}_z = \bar{\Phi}_d. \tag{2.13}$$

Thus, over one mixing event of duration $\Delta t$ (§ 2.2), the time- and volume-averaged advective buoyancy flux and irreversible diffusive flux are equal. Since we measure $\Delta E_b/\Delta t$ directly, we can infer $\bar{\Phi}_z$ from (2.5) and (2.13).

## 3. Results

We have chosen to interpret our results in terms of the parameter $\epsilon/\nu N^2$. This quantity is a convenient measure of the relative magnitude of turbulent dissipation to viscous and buoyant damping effects. Other authors have referred to the same quantity as a stratification Reynolds number (or squared ratio of the timescales of the turbulence and stratification) (Dillon & Caldwell 1980), a small-scale Froude number $Fr_\gamma^2$ (Imberger & Boashash 1986), a turbulence Reynolds number or inverse mixing efficiency (Gargett 1988), a measure of the range of overturning scales when buoyancy strongly effects the flow (Ivey *et al.* 1992), or as a strain Froude number (Imberger 1994). For simplicity, we refer to this quantity as a dimensionless measure of turbulence intensity.

### 3.1. *Turbulent lengthscale* $L_t$

The r.m.s. turbulent lengthscale $L_t$ (2.1) was directly measured (§ 2.3). The Ozmidov lengthscale, $L_o$, and the Kolmogorov lengthscale, $L_K$, were computed using measurements of $N$, $\epsilon$ and $\nu$. The definitions of these lengthscales are given, with their interpretations, in table 1. The behaviour of $L_t$, $L_o$ and $L_K$ with varying $\epsilon/\nu N^2$ is shown in figure 3 for all experiments. Horizontal lines corresponding to the grid bar size, grid mesh size and tank depth are also shown.

As seen from the figure, $L_K < L_t < L_o$ for all runs. Balmforth, Llewellyn Smith & Young (1998) argued that a natural estimate for a turbulent mixing lengthscale $l$, could be related to some characteristic dimension of the stirring device $d$. However, figure 3 shows that $L_t$ is not strongly correlated with either the mesh or bar size of the grid. Although for $\epsilon/\nu N^2 \approx 3500$ in the water experiments, $L_t$ is similar in magnitude to the grid bar size, the trend in $L_t$ over $10 < \epsilon/\nu N^2 < 10^5$ indicates that a signature of the grid bar dimension does not dominate the r.m.s. turbulent lengthscale. In particular, for $300 < \epsilon/\nu N^2 < 2500$, where we have measurements of $L_t$ from both the water and water–glycerol experiments, figure 3 shows that the

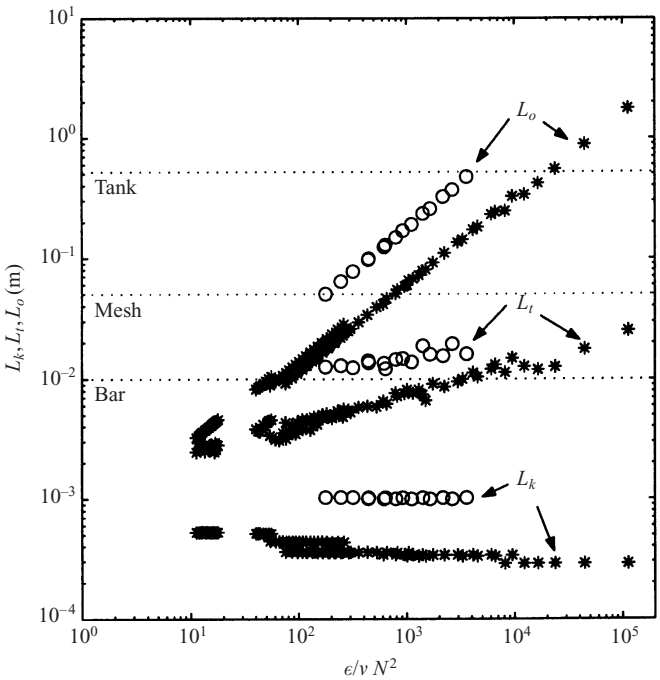


FIGURE 3. All lengthscales *vs.* turbulence intensity $\epsilon/\nu N^2$; *, water experiments; O, water–glycerol experiments. Horizontal lines correspond to the grid bar and mesh scales, and the tank depth. See table 1 for the definition of these lengthscales. The vertical temperature gradient in the final mixing events of both water–glycerol experiments was insufficient to allow computation of $L_t$.

turbulent cascades of the two fluids have distinctly different r.m.s. lengthscales for a given $\epsilon/\nu N^2$.

Figure 3 shows that for $\epsilon/\nu N^2 < 300$, the measured lengthscale data become slightly more scattered. In figures 4 and 5 we plot $L_t$ against $L_{co}$ for the two regimes where $\epsilon/\nu N^2 > 300$ and $\epsilon/\nu N^2 < 300$, respectively, where $L_{co}$ is the convective lengthscale,

$$L_{co} = \frac{(\nu\kappa)^{1/4}}{N^{1/2}}. \tag{3.1}$$

$L_{co}$ has previously been used in the analysis of decaying stratified turbulence (Pearson & Linden 1983) and stratified boundary mixing (Ivey & Corcos 1982). In the current experiments we find that $L_t$ is related to $L_{co}$,

$$L_t = 20L_{co}, \tag{3.2}$$

for $\epsilon/\nu N^2 > 300$. We refer to this regime as the energetic regime, Regime E. The convective lengthscale is related to the primitive lengthscale $L_p$ by the Prandtl number,

$$L_p = \left(\frac{\nu}{N}\right)^{1/2} = L_{co}Pr^{1/4}, \tag{3.3}$$

where $L_p$ has previously been discussed in the dynamics of stratified turbulence (e.g. Gibson 1980; Gargett 1988; Imberger 1994, 1998).

We can substitute (3.2) for $L$ into the expression for $Ra$,

$$Ra = \frac{N^2L^4}{\nu\kappa} \approx (20)^4 \approx 2 \times 10^5. \tag{3.4}$$

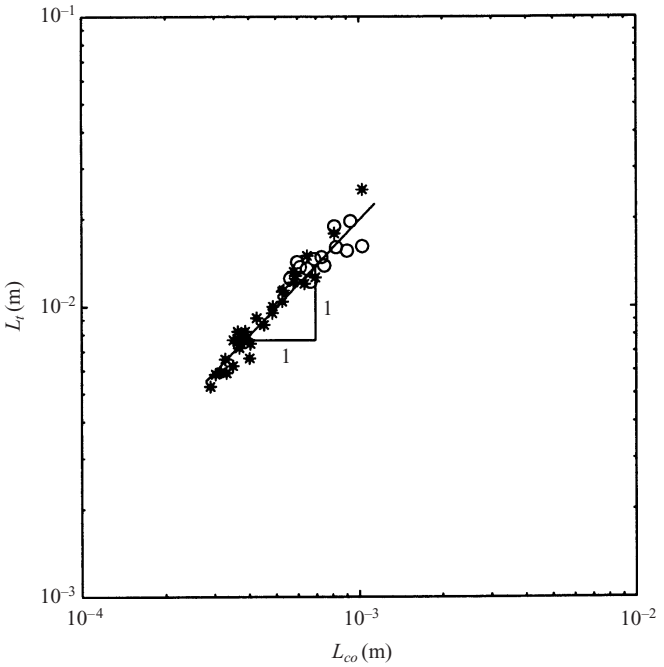


FIGURE 4. Measured r.m.s. turbulent lengthscale $L_t$ *vs.* convective lengthscale $L_{co} = (\nu\kappa)^{1/4}/N^{1/2}$ for $\epsilon/\nu N^2 > 300$; *, water experiments; O, water–glycerol experiments. The solid line is a slope 1:1 line, which has $L_t = 20L_{co}$. The line of best fit was slope 1.08, with coefficient 37.

The Rayleigh number is used to characterize the evolution of convectively driven turbulence. Although highly dependent on flow geometry and Prandtl number, convection is considered to be fully turbulent when $Ra \gtrapprox 10^5$ (Horanyi, Krebs & Müller 1999, figure 19). Hence, (3.4) suggests that in Regime E the flow is fully turbulent.

The Rayleigh number measures the relative importance of restoring buoyant effects compared to viscous and diffusive effects on a displaced fluid particle in a stratified flow (Lesieur 1997). This can be thought of in terms of the timescales characterizing the motion of such a particle,

$$Ra = \frac{T_\nu T_\kappa}{T_b^2}, \tag{3.5}$$

where $T_b$ is the timescale of return to equilibrium ($N^{-1}$), $T_\nu$ the timescale for suppression of momentum by viscosity ($L^2/\nu$) and $T_\kappa$ the timescale of smoothing of the density perturbation by molecular diffusion ($L^2/\kappa$). If $T_b$ is small compared to $T_\nu$ and $T_\kappa$, it is possible that some of the available potential energy in the density overturn will be used in mixing. The Rayleigh number is closely related to the Grashof number, $Gr = (N^2L^4)/\nu^2$, since,

$$Gr = Ra/Pr, \tag{3.6}$$

and Imberger (1994) has previously used $Gr$ to characterize turbulent fields. The Grashof number has also been interpreted in terms of the above timescales (Imberger 1994), specifically, $Gr$ is the square of the ratio of $T_\nu$ to $T_b$.

Equations (3.2) and (3.5) suggest that both $\nu$ and $\kappa$ are relevant to the dynamics of fully developed stratified turbulence. In particular, these equations suggest that a turbulent overturn in a stratified flow can lose its identity by the diffusion of both

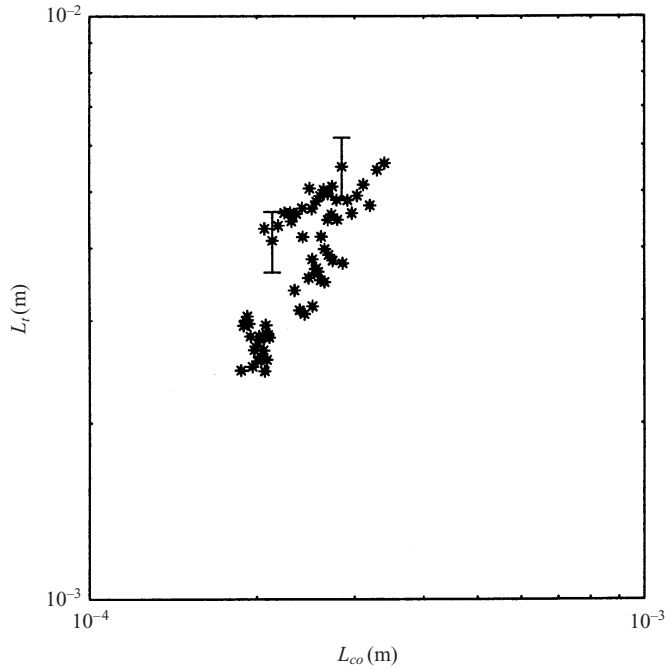


FIGURE 5. Measured r.m.s. turbulent lengthscale $L_t$ *vs.* convective lengthscale $L_{co} = (\nu\kappa)^{1/4}/N^{1/2}$ for $\epsilon/\nu N^2 < 300$. Data was only collected from the water experiments in this regime, and as such, no regression analysis has been performed on this data. There is approximately $\pm 12\%$ error in the measurements of $L_t$ and two error bars have been drawn on the figure to illustrate this.

momentum and density. Further, our observation that $Ra$ is constant in this regime may imply that there is a balance between viscous and buoyant forces, with buoyancy being lost to molecular diffusion via $\kappa$.

Equation (3.2) implies that in Regime E, $L_t$ is independent of $\epsilon$. In this regime, $\epsilon$ varied by more than one order of magnitude. Saggio & Imberger (2001) found the same result for turbulence in the thermocline of a lake for $\epsilon/\nu N^2 > 36$. We suggest that $L_{co}$ is a fundamental lengthscale of the turbulence in Regime E.

Figure 5 shows $L_t$ *vs.* $L_{co}$ for Regime W, $\epsilon/\nu N^2 < 300$. The figure indicates that $L_{co}$ is not a good predictor for the r.m.s. turbulent lengthscale in Regime W. This suggests that the turbulence has undergone a change in behaviour at $\epsilon/\nu N^2 \approx 300$. We do not have enough data in this regime to offer further quantitative analysis of our results.

### 3.2. *Turbulent diffusivity, $K_\rho$*

As a quantitative relationship between $K_\rho$ and the non-dimensional quantity $\epsilon/\nu N^2$ is sought, $K_\rho$ must be non-dimensionalized. In general, either $\kappa$ or $\nu$, or any combination of these two quantities, could be chosen to non-dimensionalize $K_\rho$ as,

$$\frac{K_\rho}{\nu^\alpha \kappa^\beta} \quad \text{with} \quad \alpha + \beta = 1. \tag{3.7}$$

In figure 6, we have plotted $K_\rho/\kappa$, $K_\rho/\nu$ and $K_\rho/(\nu^{2/3}\kappa^{1/3})$. The figure shows that normalization of $K_\rho$ by either $\kappa$ or $\nu$ does not collapse the data from the experiments with different Prandtl numbers. Figure 6(*c*), however, shows an excellent collapse.

Regardless of the normalization of $K_\rho$, we note the following from figure 6. First, the figure demonstrates a smooth evolution of $K_\rho$ over more than four orders of

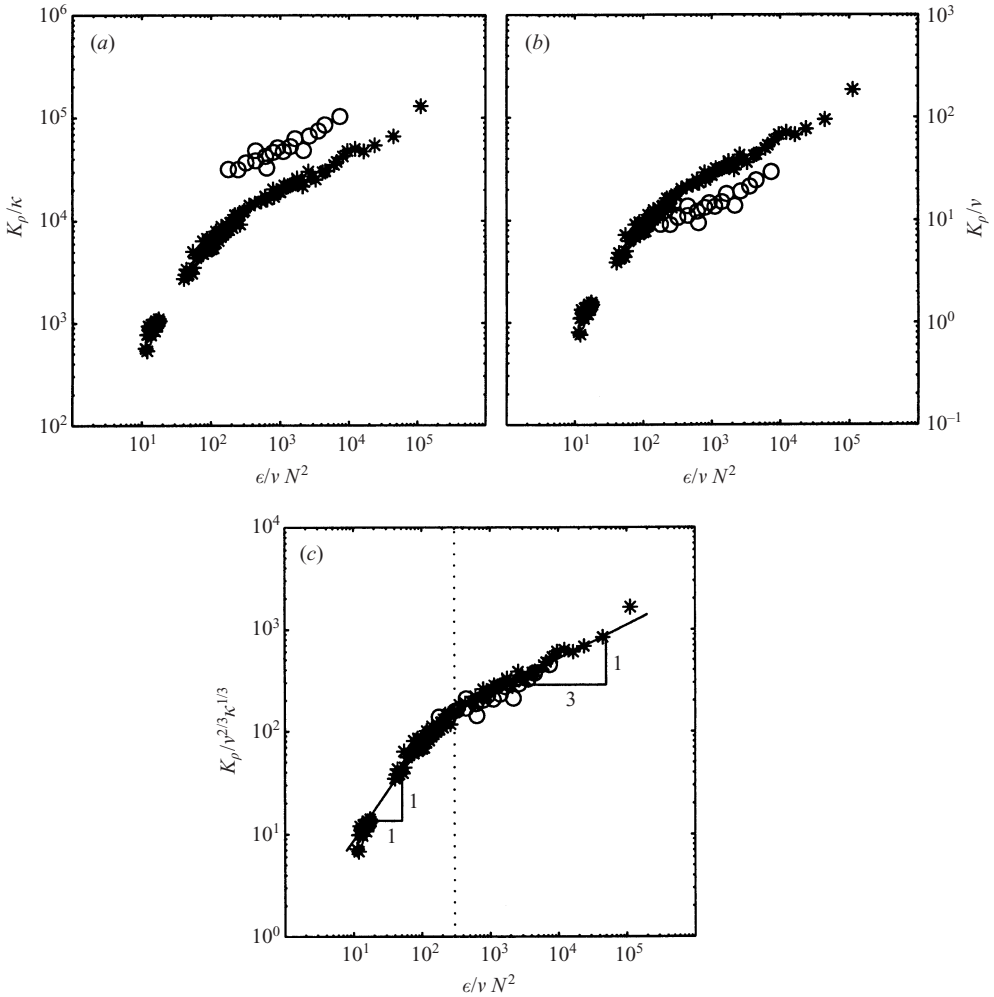


FIGURE 6. Comparison of the normalization of $K_\rho$ by (*a*) $\kappa$, (*b*) $\nu$ and (*c*) $\nu^{2/3}\kappa^{1/3}$; *, water experiments; O, water–glycerol experiments. In all cases, the normalized $K_\rho$ is plotted against the turbulence intensity $\epsilon/\nu N^2$. The solid lines in (*c*) are of slope 1 and 1/3. The best-fit lines were of slopes 0.91 and 0.35, respectively. The vertical dotted line in (*c*) is at $\epsilon/\nu N^2 = 300$, and delineates the transition point between Regime E ($\epsilon/\nu N^2 > 300$) and Regime W ($\epsilon/\nu N^2 < 300$).

magnitude of $\epsilon/\nu N^2$. Secondly, even for the smallest turbulence intensity $\epsilon/\nu N^2 = 10$, $K_\rho$ is approximately three orders of magnitude greater than the molecular diffusivity. By using (2.13), we infer that the time- and volume-averaged vertical advective flux in these experiments is non-zero at $\epsilon/\nu N^2 \approx 15$, and that $K_\rho$ does not vanish at $\epsilon/\nu N^2 \approx 15$.

The lengthscale analysis suggests that at $\epsilon/\nu N^2 \approx 300$ there is a change in behaviour of the turbulence. Figure 6(*c*) shows that the turbulent diffusivity data are also separable into two regimes, with the division between these regimes also at $\epsilon/\nu N^2 \approx 300$. We refer to these regimes as Regimes E and W, as before.

From figure 6(*c*) our collapsed data show that in Regime E,

$$K_\rho = 24\nu^{2/3}\kappa^{1/3}\left(\frac{\epsilon}{\nu N^2}\right)^{1/3}, \tag{3.8}$$

with correlation coefficient $r^2 = 0.97$. We note that this expression for $K_\rho$ results from our choice to normalize $K_\rho$ by $\nu^{2/3}\kappa^{1/3}$. This choice was motivated by the form of $K_\rho$ obtained by substituting (3.1) as a scale estimate for $L_t$ into (1.3). This substitution predicts that,

$$K_\rho \sim \nu^{2/3}\kappa^{1/3}\left(\frac{\epsilon}{\nu N^2}\right)^{1/3}, \tag{3.9}$$

which is precisely the form of $K_\rho$ that collapses our diffusivity data.

We do not have data in Regime W for the water–glycerol experiments. The turbulent diffusivity from the water experiments is attenuated throughout Regime W and this again suggests that the turbulence has undergone a transition in character. This transition manifests itself in the turbulent diffusivity measurements for $\epsilon/\nu N^2 < 300$, where the power dependence on $\epsilon/\nu N^2$ deviates from one third. We fit a linear regression to the diffusivity data in Regime W,

$$K_\rho = 0.9\nu^{2/3}\kappa^{1/3}\left(\frac{\epsilon}{\nu N^2}\right). \tag{3.10}$$

We note that this fit has the same functional dependence on $\epsilon/N^2$ as the model of Osborn (1980), however, (3.10) has a different constant coefficient to (1.10) and also includes the influence of molecular diffusivity on turbulent mixing.

### 3.3. *Turbulent r.m.s. velocity scale, $U_t$*

Given (3.2) and (3.8), we have used (1.1) to predict a time- and volume-averaged r.m.s. turbulent velocity scale, $U_t$ in Regime E,

$$U_t \sim \left(\frac{\epsilon}{\nu N^2}\right)^{1/3}\nu^{5/12}\kappa^{1/12}N^{1/2} \sim \left(\frac{\epsilon}{\nu N^2}\right)^{1/3}(\nu N)^{1/2}Pr^{-1/12}. \tag{3.11}$$

We note the weak dependence of $U_t$ on both $\nu$ and $\kappa$. We can compare our prediction for $U_t$ with other data sets. Saggio & Imberger (2001) measured a turbulent velocity scale directly in the metalimnion of a freshwater lake. They found that for $\epsilon/\nu N^2 > 36$,

$$U_t = 3.0\left(\frac{\epsilon}{\nu N^2}\right)^{1/3}(\nu N)^{1/2}, \tag{3.12}$$

which can be rewritten in a form consistent with (3.11) as,

$$U_t = 3.5\left(\frac{\epsilon}{\nu N^2}\right)^{1/3}(\nu N)^{1/2}Pr^{-1/12}. \tag{3.13}$$

Similarly, Itsweire *et al.* (1986) measured streamwise ($u'$) and vertical ($w'$) velocity fluctuations directly in their salt stratified water tunnel experiments. We have plotted these data in figures 7(*a*) and 7(*b*), respectively. The figures show that for $\epsilon/\nu N^2 > 100$ (of which $\epsilon/\nu N^2 > 300$ is a subset),

$$\frac{u'}{\{(\nu N)^{1/2}Pr^{-1/12}\}} = 3.6(\epsilon/\nu N^2)^{1/3}, \tag{3.14a}$$

$$\frac{w'}{\{(\nu N)^{1/2}Pr^{-1/12}\}} = 2.8(\epsilon/\nu N^2)^{1/3}, \tag{3.14b}$$

where the lines of best fit resulted in powers of 0.32 and 0.33 for $\epsilon/\nu N^2$, with correlation coefficients of 0.98 and 0.96, respectively. These are again of the same form as (3.11). The scatter in the Itsweire *et al.* (1986) data increases for $\epsilon/\nu N^2 < 100$, suggesting that the scaling in (3.11) no longer holds. This is consistent with a change in the character of the turbulence for $\epsilon/\nu N^2 < 300$.

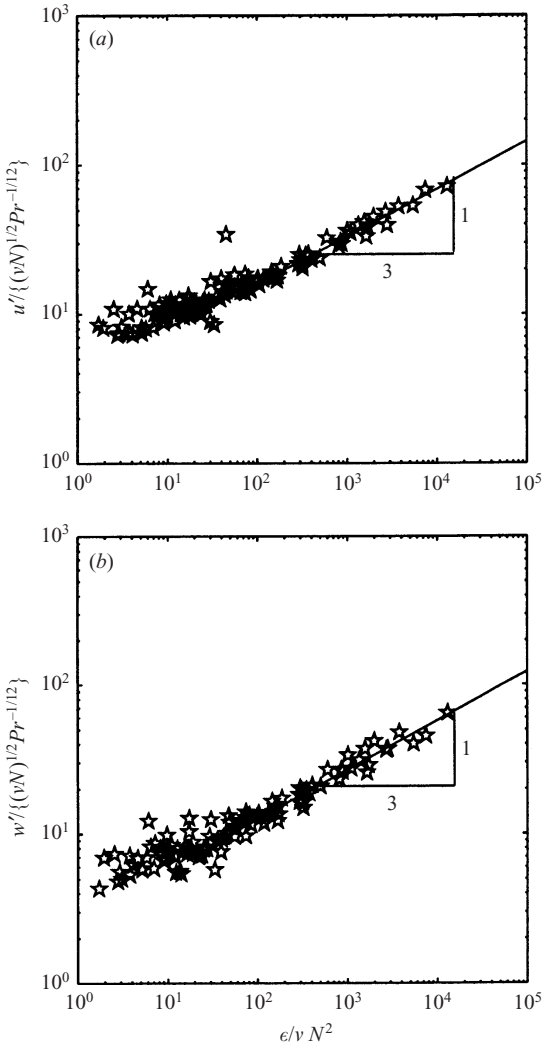


FIGURE 7. Normalized streamwise and vertical turbulent velocity fluctuations from the data of Itsweire *et al.* (1986): (*a*) $u'/\{(\nu N)^{1/2}Pr^{-1/12}\}$ *vs.* turbulence intensity $\epsilon/\nu N^2$; (*b*) $w'/\{(\nu N)^{1/2}Pr^{-1/12}\}$ *vs.* turbulence intensity $\epsilon/\nu N^2$. The solid lines represent the form of our scale prediction for the r.m.s. velocity scale, $U_t/\{(\nu N)^{1/2}Pr^{-1/12}\} \sim (\epsilon/\nu N^2)^{1/3}$ for $\epsilon/\nu N^2 > 100$.

We note that under our suggested velocity scaling, there is little variation in the constant coefficient between field (heat stratified) and laboratory (salt stratified) data sets. Taking an average of the coefficients in (3.13) and (3.14*a*, *b*), we suggest that in Regime E,

$$U_t = 3.3\left(\frac{\epsilon}{\nu N^2}\right)^{1/3}(\nu N)^{1/2}Pr^{-1/12}. \tag{3.15}$$

Since we were unable to quantitatively describe the behaviour of $L_t$ for $\epsilon/\nu N^2 < 300$ we cannot infer a velocity scale from our data in Regime W.

## 4. Discussion

### 4.1. *An interpretation of the mechanism of turbulent mixing*

We have expressed $K_\rho$ as a product of a turbulent velocity scale $U_t$ and turbulent lengthscale $L_t$, and for $\epsilon/\nu N^2 > 300$,

$$\underbrace{\left\{\nu^{2/3}\kappa^{1/3}\left(\frac{\epsilon}{\nu N^2}\right)^{1/3}\right\}}_{K_\rho} \sim \underbrace{\left\{\left(\frac{\epsilon}{\nu N^2}\right)^{1/3}(\nu N)^{1/2}Pr^{-1/12}\right\}}_{U_t}\underbrace{\left\{\frac{(\nu\kappa)^{1/4}}{N^{1/2}}\right\}}_{L_t}. \tag{4.1}$$

This scale expression suggests an interpretation of the response of a turbulent cascade to a change in the rate of supply of turbulent energy. For a given buoyancy frequency $N$, and for a flow satisfying $\epsilon/\nu N^2 > 300$, (4.1) shows that whilst the r.m.s. turbulent velocity changes with the one third power of $\epsilon$, $L_t$ remains unchanged. This implies that, at least instantaneously, the turbulent cascade responds to a change in the rate of energy supply not by altering the r.m.s. lengthscale, but by modifying the r.m.s. velocity of the turbulent overturns. Thus, for a change in turbulence intensity, we predict $K_\rho$ will also change, not via an adjustment of the r.m.s. turbulent lengthscale $L_t$, but rather through modification of the r.m.s. turbulent velocity scale $U_t$.

We suggest that this change in $U_t$ gives rise to a change in the rate of strain of isopycnal surfaces at the small scales, and hence a change in the irreversible diffusive flux, $\Phi_d$. Winters & D'Asaro (1996) argue that such a change in $\Phi_d$ will result in a corresponding change in $K_\rho$. This interpretation of the mechanism of turbulent mixing is consistent with our result in (4.1).

Balmforth *et al.* (1998) argued that the vertical mass flux in a stratified turbulent fluid may depend on the manner in which energy is supplied to the flow. Since we have not varied the forcing mechanism in the current experiments, we are not in a position to assess this argument and relate it to our interpretation of (4.1).

### 4.2. *Comparison with prior models of turbulent mixing*

It is useful to recast our results in terms of prior models for $K_\rho$. Of particular interest is the comparison between our results and the prediction of $K_\rho$ due to Osborn (1980),

$$K_\rho \leqslant 0.2\left(\frac{\epsilon}{N^2}\right), \tag{4.2a}$$

i.e.

$$\frac{K_\rho}{\nu^{2/3}\kappa^{1/3}} \leqslant 0.2\frac{1}{\nu^{2/3}\kappa^{1/3}}\left(\frac{\epsilon}{N^2}\right) = 0.2\frac{\epsilon}{\nu N^2}Pr^{1/3}. \tag{4.2b}$$

In order to compare the prediction of Osborn (1980) with our results, we have used values of $Pr = 7$ (temperature stratified water) and $Pr = 700$ (salt stratified water) in (4.2*b*). Figure 8 shows normalized diffusivities from the current experiments, and $K_\rho/\nu^{2/3}\kappa^{1/3}$ predicted from (4.2*b*) with $Pr = 700$ and 7 shown as solid and dotted lines, respectively.

Our results show that the magnitude of the diffusivity predicted by the Osborn (1980) model is similar to our direct measurements only for $10 < \epsilon/\nu N^2 < 1000$. In this range, and with $Pr = 7$, (4.2) is within a factor of 2 of the diffusivity measured in these experiments. However, with $Pr = 700$, (4.2*b*) overpredicts $K_\rho$ by a factor of approximately 2.5 over this entire range. For $\epsilon/\nu N^2 > 1000$, (4.2*b*) is an overestimate of the measured $K_\rho$ for both $Pr = 7$ and 700. When $\epsilon/\nu N^2 \approx 10^4$, (4.2*b*) is, at best, one order of magnitude greater than the experimental results. Hence, our results suggest that the application of the model of Osborn (1980) to highly energetic geophysical

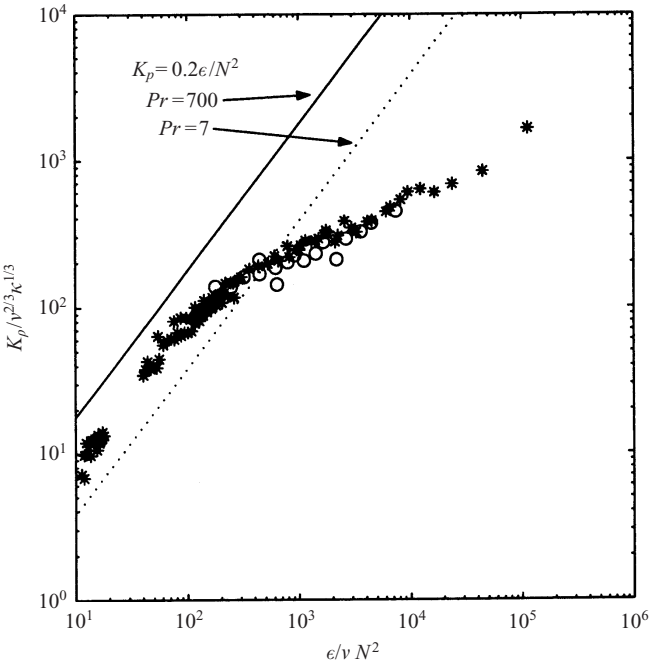


FIGURE 8. Normalized experimental diffusivity results, $K_\rho/\nu^{2/3}\kappa^{1/3}$ and the normalized prediction for $K_\rho$ due to Osborn (1980) *vs.* turbulence intensity $\epsilon/\nu N^2$; *, water experiments; O, water–glycerol experiments; —, Osborn (1980), for $Pr = 700$; $\cdots$, Osborn (1980), for $Pr = 7$.

flows (e.g. Ferron *et al.* 1998, in the Romanche fracture zone where $\epsilon/\nu N^2 \approx 500\,000$) may lead to an overprediction of $K_\rho$.

The derivation of (4.2*b*) assumes a steady-state homogeneous turbulent kinetic energy balance, defines $K_\rho$ in terms of the advective buoyancy flux $b$, and assumes an approximately constant flux Richardson number, $R_f = -b/S_p$ of 0.15 (§ 1.2). The current experiments were executed such that the first two assumptions were close to being satisfied (§ 2.6). We conclude then that the choice of $R_f$ as a constant is likely to be the primary cause of the divergence between (4.2*b*) and the measured $K_\rho$ for $\epsilon/\nu N^2 > 1000$.

By analysing laboratory data, Ivey & Imberger (1991) suggested that the mixing efficiency $R_f$ can be written as a function of $\epsilon, N^2$ and some turbulent lengthscale $L$ in (1.9). Substituting their expression for $R_f$ (their equation 20) for Regime E into (1.9) leaves,

$$K_\rho \sim \frac{N^2 L_C^{4/3}}{\epsilon^{2/3}} \frac{\epsilon}{N^2} \sim \epsilon^{1/3} L_C^{4/3}, \tag{4.3}$$

where $L_C$ is a centred displacement scale describing the scale of the turbulent overturns. This expression is of precisely the same form as we have used in our analysis of $K_\rho$ in Regime E. Therefore, an interpretation of our results in § 3, and one that is consistent with the results of Ivey & Imberger (1991) and Ivey *et al.* (1998), is that $R_f$ is not constant for all $\epsilon/\nu N^2$. However, using a formulation for $K_\rho$ involving $R_f$ requires knowledge of $\epsilon, N^2$ and $L_C$. By using (3.8) (or (3.10)), $K_\rho$ can be evaluated directly from only $\epsilon$ and $N^2$, without knowledge of a turbulent lengthscale.

## 5. Conclusions

Using fluids of different Prandtl number, we have undertaken controlled laboratory experiments that have directly and independently measured both a time- and volume-averaged r.m.s. turbulent lengthscale, $L_t$, and turbulent diffusivity for mass, $K_\rho$. We have expressed these quantities as functions of the rate of dissipation of turbulent kinetic energy $\epsilon$, stratification strength $N^2$, and Prandtl number $Pr$, which were also directly measured as time- and volume-averaged quantities. The turbulence intensity $\epsilon/\nu N^2$, was varied such that $10 < \epsilon/\nu N^2 < 10^5$. The results show that the behaviour of both $L_t$ and $K_\rho$ can be distinguished by the magnitude of this turbulence intensity. We identified two such regimes.

In the energetic regime (Regime E), where $300 < \epsilon/\nu N^2 < 10^5$, $L_t$ and $K_\rho$ are described by,

$$L_t = 20\frac{(\nu\kappa)^{1/4}}{N^{1/2}}, \tag{5.1a}$$

$$K_\rho = 24\nu^{2/3}\kappa^{1/3}\left(\frac{\epsilon}{\nu N^2}\right)^{1/3}. \tag{5.1b}$$

Whilst not measuring an r.m.s. velocity scale directly, we computed an expression for this quantity from (5.1$a$, $b$) in Regime E,

$$U_t = 3.3\left(\frac{\epsilon}{\nu N^2}\right)^{1/3}(\nu N)^{1/2}Pr^{-1/12}. \tag{5.2}$$

The scale form of the predictions (5.1$a$, $b$) and (5.2) are consistent with theoretical predictions and laboratory and field measurements. The constant coefficient in (5.2) has been estimated from field and laboratory data.

$K_\rho$ was decomposed into a product of turbulent length and velocity scales and this facilitated an alternative interpretation of the mechanism by which irreversible mixing may occur in Regime E. In stratified turbulence, we suggest that for a given $N$, and an increase in the turbulence intensity, the corresponding increase in diffusivity is not accomplished by an increase in the distance over which mass is transferred by turbulent overturns, as $L_t$ is not a function of $\epsilon$. Rather, we suggest that the corresponding increase in the turbulent velocity $U_t$ gives rise to an increase in the rate of strain of isopycnal surfaces at the small scales, and hence an increase in the small-scale diffusive, or irreversible, mass flux.

In the weaker regime (Regime W) where $10 < \epsilon/\nu N^2 < 300$, the relationships for $L_t$, $K_\rho$ and $U_t$ in Regime E do not hold. We suggest that at $\epsilon/\nu N^2 \approx 300$ in these experiments, the turbulence undergoes a change in character, with a corresponding change in the behaviour of $L_t$ and $K_\rho$. In regime W we found that,

$$K_\rho = 0.9\nu^{2/3}\kappa^{1/3}\left(\frac{\epsilon}{\nu N^2}\right). \tag{5.3}$$

We were unable to identify quantitative expressions for $L_t$ or $U_t$ for $\epsilon/\nu N^2 < 300$. We have identified a similar transition point between Regimes E and W in other field and laboratory data sets. Below this transition point, an alternative model of the turbulence is required to understand fully the dynamics of the flow.

We have compared our diffusivity results with the prediction of Osborn (1980) for heat and salt stratified fluids. For $\epsilon/\nu N^2 < 1000$ there is up to approximately a factor of 2 difference between this prediction and the measured turbulent diffusivity for $Pr = 7$. Above this range, the prediction of Osborn (1980) for both $Pr = 7$ and 700 diverges from the measurements of $K_\rho$ in these experiments. We suggest that

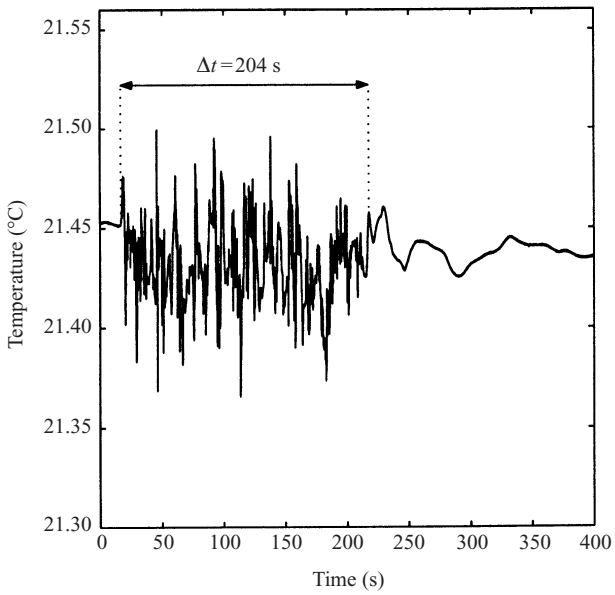


FIGURE 9. Temperature (°C) *vs.* time (s) for a typical time series taken from a stationary thermistor during a mixing event. Three sections can be identified: quiescent fluid before the initiation of grid stirring; turbulence during grid stirring; and the decay of internal waves after stirring has ceased.

this may be a result of forcing $K_\rho$ to depend on $\epsilon/N^2$, and selecting a constant flux Richardson number.

The authors wish to thank David Horn, Jason Antenucci, Graham Hughes and the anonymous reviewers for providing valuable comments on an initial draft of this manuscript. Charles Apro, Wladek Bzdyl, Sun Nickerson and Bill Deugd provided technical expertise to assist with construction and maintenance of the laboratory apparatus and instrumentation. M. B. was supported by an Australian Postgraduate Award and a Samaha Research Scholarship. This forms Centre for Water Research reference ED1560-MB.

## Appendix. Subsidiary measurements: $\Delta t$, $F_D$, $\mathrm{d}\rho/\mathrm{d}z$ and $\nu$

### A.1. *Measurement of* $\Delta t$

The measurement of $\Delta t$ was accomplished in two ways. First, an electronic stopwatch was used to take the time from the commencement to termination of grid motion over a mixing event. This measurement provided a first-order approximation to the active mixing time $\Delta t$.

The horizontally oriented thermistors collected turbulent temperature time series during a mixing event. Figure 9 shows a typical time series and the corresponding $\Delta t$. Three sections can be clearly identified in this time series: the quiescent fluid prior to the commencement of grid motion, the turbulent section during grid motion, and the decay of internal waves after the grid has ceased motion.

From this typical record, the duration of the turbulent section was extracted and used as the active mixing time, $\Delta t$. This time was usually within 5% of the time measured on the laboratory stopwatch. The turbulent mixing times extracted from each of the two stationary thermistors were averaged to give a single estimate of $\Delta t$.

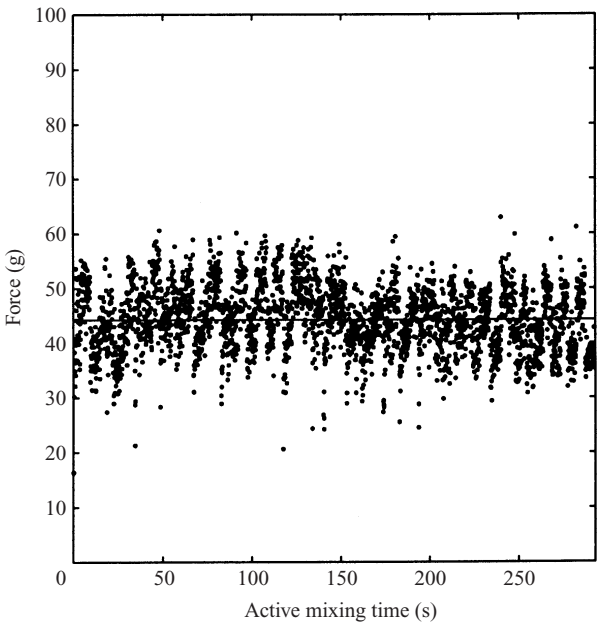


FIGURE 10. Measured force (g) *vs.* active mixing time (s) for a typical processed force transducer record; ·, instantaneous force measurement; —, mean force. The measurement of force in grams was converted to Newtons using $F = mg$, as per manufacturers specifications.

We note that the thermistor record shows some oscillatory motion which may be related to the grid return timescale. We have removed this behaviour by computing and considering only time- and volume-averaged $L_t$ and $K_\rho$. We offer no insight into the temporal evolution of these quantities within a given mixing event.

Some internal wave activity is also evident in the temperature time series (e.g. figure 9). By filtering, we extracted the components of the time series due only to internal waves. We then found the maximum observed internal wave displacement, and using linear internal wave theory (see Kundu 1990, pp. 244–245 for example), found that the total energy associated with the observed internal wave field is typically less than 0.5% of the work done by the grid on the fluid.

### A.2. *Measurement of* $F_D$

To compute a time- and volume-averaged drag force, $F_D$ was measured continuously during a mixing event. As the grid touched the tank at the end of each traverse, the force logged during that time (usually in the order of 0.2 s) was not representative of the true drag force. As a result, these sections of the record were removed and the average of the magnitude of the remainder of the record was taken as the drag force $F_D$. Figure 10 shows a typical force time series (with the mean $F_D$) processed in this manner.

The processed force transducer signal shows some noise over the mean signal. This is due to a slight jerkiness in the power supplied by the pneumatic drive.

### A.3. *Measurement of* $\mathrm{d}\rho/\mathrm{d}z$

To maintain consistency with other measurements, the background density gradient was again computed as a time- and volume-averaged quantity. For a given mixing event, a pair of vertical FRC/FP07 profiles was taken before and after mixing. Each

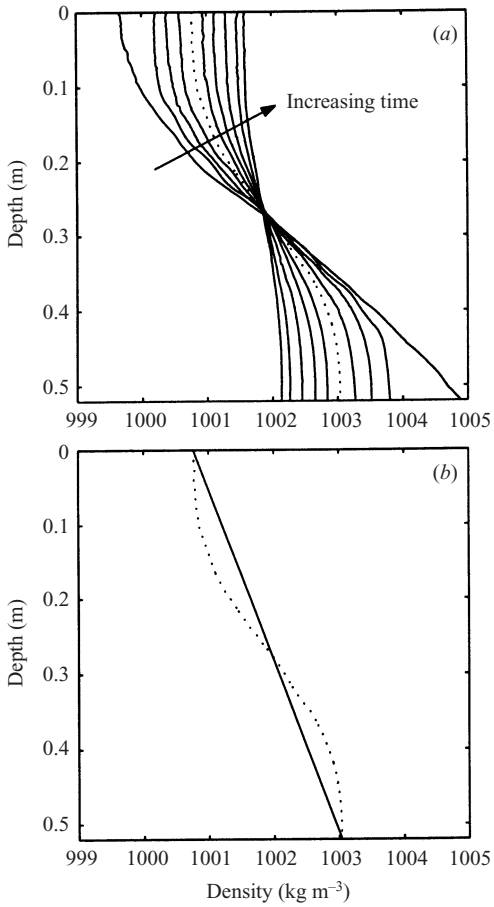


FIGURE 11. (*a*) Depth (m) *vs.* density (kg m$^{-3}$) evolving in time for a typical experiment. The dotted profile in (*a*) is repeated in (*b*) with the linear density profile used to compute $N^2$ superimposed (see § A.1).

of the two pairs of profiles was averaged to give a single representative profile before and after mixing. These two profiles were then averaged in time across the mixing event to give a single time-averaged density profile. From this, a volume-averaged density gradient was computed as,

$$\frac{\mathrm{d}\rho}{\mathrm{d}z} = \frac{\rho_{top} - \rho_{base}}{H}, \tag{A 1}$$

where $H$ is the depth of fluid. This gives a time and volume averaged $\mathrm{d}\rho/\mathrm{d}z$.

Owing to practical sampling issues, the vertical FRC profiles were unable to measure density over the entire depth of the fluid. As a result, the profiles were extrapolated to the fluid surface and tank bottom. The total height over which the profiles were extrapolated was less than 5 mm. Figure 11(*a*) shows a typical evolution of the density profile with depth over the course of several mixing events. Figure 11(*b*) shows one of the profiles from figure 11(*a*) overlaid with the linear density profile used to compute $N^2$ from § A.1.

## REFERENCES


Balmforth, N. J., Llewellyn Smith, S. G. & Young, W. R. 1998 Dynamics of interfaces and layers in a stratified turbulent fluid. *J. Fluid Mech.* **355**, 329–358.

Dillon, T. M. & Caldwell, D. R. 1980 The Batchelor spectrum and dissipation in the upper ocean. *J. Geophys. Res.* **85**, 1910–1916.

Ellison, T. H. 1957 Turbulent transport of heat and momentum from an infinite rough plane. *J. Fluid Mech.* **2**, 456–466.

Ferron, B., Mercier, H., Speer, K., Gargett, A. & Polzin, K. 1988 Mixing in the Romanche Fracture Zone. *J. Phys. Oceanogr.* **28**, 1929–1945.

Gargett, A. E. 1988 The scaling of turbulence in the presence of stable stratification. *J. Geophys. Res.* **93**, 5021–5036.

Gibson, C. H. 1980 Fossil temperature, salinity and vorticity turbulence in the ocean. In *Marine Turbulence* (ed. J. C. T. Nihoul), pp. 221–257. Elsevier.

Holford, J. M. & Linden, P. F. 1999 Turbulent mixing in a stratified fluid. *Dyn. Atmos. Oceans* **30**, 173–198.

Horanyi, S., Krebs, L. & Müller, U. 1999 Turbulent Rayleigh–Bénard convection in low Prandtl number fluids. *Intl J. Heat Mass Transfer* **42**, 3983–4003.

Imberger, J. 1994 Transport processes in lakes: a review. In *Limnology Now: A Paradigm of Planetary Problems* (ed. R. Margalef), pp. 99–193. Elsevier Science.

Imberger, J. 1998 Flux paths in a stratified lake: a review. In *Physical Processes in Lakes and Oceans* (ed. J. Imberger), *Coastal and Estuarine Studies*, vol. 54, pp. 1–18. American Geophysical Union.

Imberger, J. & Boashash, B. 1986 Application of the Wigner–Ville distribution to temperature gradient microstructure: a new technique to study small-scale variations. *J. Phys. Oceanogr.* **16**, 1997–2012.

Itsweire, E. C., Helland, K. N. & Van Atta, C. W. 1986 The evolution of grid-generated turbulence in a stably stratified fluid. *J. Fluid Mech.* **162**, 299–338.

Ivey, G. N. & Corcos, G. M. 1982 Boundary mixing in a stratified fluid. *J. Fluid Mech.* **121**, 1–26.

Ivey, G. N. & Imberger, J. 1991 On the nature of turbulence in a stratified fluid. Part I: The energetics of mixing. *J. Phys. Oceanogr.* **21**, 650–658.

Ivey, G. N., Imberger, J. & Koseff, J. R. 1998 Buoyancy fluxes in a stratified fluid. In *Physical Processes in Lakes and Oceans* (ed. J. Imberger), *Coastal and Estuarine Studies*, vol. 54, pp. 377–388. American Geophysical Union.

Ivey, G. N., Koseff, J. R., Briggs, D. A. & Ferziger, J. H. 1992 Mixing in a stratified shear flow: energetics and sampling. *Center for Turbulence Research Annual Research Briefs*, pp. 335–344.

Ivey, G. N. & Nokes, R. I. 1989 Vertical mixing due to the breaking of critical internal waves on sloping boundaries. *J. Fluid Mech.* **204**, 479–500.

Ivey, G. N., Winters, K. B. & De Silva, I. P. D. 2000 Turbulent mixing in a sloping benthic boundary layer energized by internal waves. *J. Fluid Mech.* **418**, 59–76.

Kundu, P. K. 1990 *Fluid Mechanics.* Academic.

Ledwell, J. R., Montgomery, E. T., Polzin, K. L., St Laurent, L. C., Schmitt, R. W. & Toole, J. M. 2000 Evidence for enhanced mixing over rough topography in the abyssal ocean. *Nature* **403**, 179–182.

Ledwell, J. R., Watson, A. J. & Law, C. S. 1993 Evidence for slow mixing across the pycnocline from an open-ocean tracer-release experiment. *Nature* **364**, 701–703.

Lesieur, M. 1997 *Turbulence in Fluids*, 3rd edn. Kluwer.

Lienhard, J. H. & Van Atta, C. W. 1990 The decay of turbulence in thermally stratified flow. *J. Fluid Mech.* **210**, 57–112.

Liu, H.-T. 1995 Energetics of grid turbulence in a stably stratified fluid. *J. Fluid Mech.* **296**, 127–157.

Monin, A. S. & Yaglom, A. M. 1971 *Statistical Fluid Mechanics: Mechanics of Turbulence.* MIT Press.

Moum, J. N. 1990 The quest for $K_\rho$ – Preliminary results from direct measurements of turbulent fluxes in the ocean. *J. Phys. Oceanogr.* **20**, 1980–1984.

Moum, J. N. 1996 Efficiency of mixing in the main thermocline. *J. Geophys. Res.* **101**, 12 057–12 069.

Osborn, T. R. 1980 Estimates of the local rate of vertical diffusion from dissipation measurements. *J. Phys. Oceanogr.* **10**, 83–89.

Park, Y.-G., Whitehead, J. A. & Gnanadeskian, A. 1994 Turbulent mixing in stratified fluids: layer formation and energetics. *J. Fluid Mech.* **279**, 279–311.

Pearson, H. J. & Linden, P. F. 1983 The final stage of decay of turbulence in stably stratified fluid. *J. Fluid Mech.* **134**, 195–203.

Polzin, K. L., Toole, J. M., Ledwell, J. R. & Schmitt, R. W. 1997 Spatial variability of turbulent mixing in the abyssal ocean. *Science* **276**, 93–96.

Rehmann, C. R. 1995 Effects of stratification and molecular diffusivity on the mixing efficiency of decaying grid turbulence. PhD thesis, Department of Civil Engineering, Stanford University, California, USA.

Richardson, L. F. 1926 Atmospheric diffusion shown on a distance-neighbour graph. *Proc. R. Soc. Lond.* A **110**, 709–737.

Rohr, J. J., Itsweire, E. C., Helland, K. N. & Van Atta, C. W. 1988 Growth and decay of turbulence in a stably stratified shear flow. *J. Fluid Mech.* **195**, 77–111.

Ruddick, B. R., McDougall, T. J. & Turner, J. S. 1989 The formation of layers in a uniformly stirred density gradient. *Deep-Sea Res.* **36**, 597–609.

Ruddick, B. R. & Shirtcliffe, T. G. L. 1979 Data for double diffusers: physical properties of aqueous salt–sugar solutions. *Deep-Sea Res.* **26A**, 775–787.

Saggio, A. & Imberger, J. 2001 Mixing and turbulent fluxes in the metalimnion of a stratified lake. *Limnol. Oceanogr.* **46**, 392–409.

Stillinger, D. C., Helland, K. N. & Van Atta, C. W. 1983 Experiments on the transition of homogeneous turbulence to internal waves in a stratified fluid. *J. Fluid Mech.* **131**, 91–122.

Stull, R. B. 1994 *An Introduction to Boundary Layer Meteorology*. Kluwer.

Taylor, G. I. 1935 Statistical theory of turbulence. *Proc. R. Soc. Lond.* A **151**, 421.

Tennekes, H. & Lumley, J. L. 1972 *A First Course in Turbulence*. MIT Press.

Teoh, S. G., Ivey, G. N. & Imberger, J. 1997 Laboratory study of the interactions between two internal wave rays. *J. Fluid Mech.* **336**, 91–122.

Winters, K. B. & D'Asaro, E. A. 1996 Diascalar flux and the rate of fluid mixing. *J. Fluid Mech.* **317**, 179–193.

Winters, K. B. & Ivey, G. N. 1999 Turbulent properties in a wave energised benthic boundary layer on a slope. In *'Aha Huliko'a Hawaiian Winter Workshop on Dynamics of Oceanic Internal Gravity Waves, Part 2. Honolulu, Hawaii.* (ed. P. Müller & D. Henderson), pp. 149–154. School of Ocean and Earth Science Special Publication.

Winters, K. B., Lombard, P. N., Riley, J. J. & D'Asaro, E. A. 1995 Available potential energy and mixing in density-stratified fluids. *J. Fluid Mech.* **289**, 115–128.

Wuest, A., van Senden, D. C., Imberger, J., Piepke, G. & Gloor, M. 1996 Comparison of diapycnal diffusivity measured by tracer and microstructure techniques. *Dyn. Atmos. Oceans* **24**, 27–39.